Barriers for Lateral Diffusion of Transferrin Receptor in the Plasma Membrane as Characterized by Receptor Dragging by Laser Tweezers: Fence versus Tether

Yasushi Sako and Akihiro Kusumi

Department of Life Sciences, Graduate School of Arts and Sciences, The University of Tokyo, Meguro-ku, Tokyo 153, Japan

Abstract. Our previous results indicated that the plasma membrane of cultured normal rat kidney fibroblastic cell is compartmentalized for diffusion of receptor molecules, and that long-range diffusion is the result of successive intercompartmental jumps (Sako, Y. and Kusumi, A. 1994. *J. Cell Biol.* 125:1251–1264). In the present study, we characterized the properties of intercompartmental boundaries by tagging transferrin receptor (TR) with either 210-nm-ϕ latex or 40-nm-ϕ colloidal gold particles, and by dragging the particle–TR complexes laterally along the plasma membrane using laser tweezers. Approximately 90% of the TR–particle complexes showed confined-type diffusion with a microscopic diffusion coefficient (D_{micro}) of $\sim 10^{-9}$ cm^2/s and could be dragged past the intercompartmental boundaries in their path by laser tweezers at a trapping force of 0.25 pN for gold-tagged TR and 0.8 pN for latex-tagged TR. At lower dragging forces between 0.05 and 0.1 pN, particle–TR complexes tended to escape from the laser trap at the boundaries, and such escape occurred in both the forward and backward directions of dragging. The average distance dragged was half of the confined distance of TR, which further indicates that particle–TR complexes escape at the compartment boundaries. Since variation in the particle size (40 and 210 nm, the particles are on the extracellular surface of the plasma membrane) hardly affects the diffusion rate and behavior of the particle–TR complexes at the compartment boundaries, and since treatment with cytochalasin D or vinblastin affects the movements of TR (Sako and Kusumi as cited above), argument has been advanced that the boundaries are present in the cytoplasmic domain. Rebound of the particle–TR complexes when they escape from the laser tweezers at the compartment boundaries suggests that the boundaries are elastic structures. These results are consistent with the proposal that the compartment boundaries consist of membrane skeleton or a membrane-associated part of the cytoskeleton (membrane skeleton fence model). Approximately 10% of TR exhibited slower diffusion (D_{micro} $\sim 10^{-10}$–10^{-11} cm^2/s) and binding to elastic structures.

RECENT development of single particle tracking (SPT)[1] by nanovid microscopy has made it possible to observe the movements of individual (or a small number of) membrane receptor molecules by labeling proteins with colloidal gold particles (20–40 nm in diameter) on the living cell surface using video-enhanced contrast microscopy (De Brabander et al., 1985, 1986; Geerts et al., 1987, 1991) with a possibility of nanometer spatial precision (Gelles et al., 1988; Schnapp et al., 1988; Kucik et al, 1989; Sheetz et al., 1989). The SPT method is unique in that it can reveal the mechanisms by which motion of a single protein molecule is regulated in the plasma membrane. The nanometer-level precision of SPT is particularly useful for studying regulation mechanisms that act at the submicron scale, such as the membrane skeleton (Kusumi et al., 1993; Sako and Kusumi, 1994). Various methods for analyzing SPT data have been developed (Qian et al., 1991; Kusumi et al., 1993; Saxton, 1993). Fluorescence SPT has also been developed (Anderson et al., 1992; Ghosh and Webb, 1994).

Previous SPT studies have suggested that the plasma membranes of a variety of animal cells, such as normal rat kidney fibroblastic (NRK) cells, mouse keratinocytes, and human erythrocytes, are compartmentalized into many small domains of 0.01–0.25 μm^2 (depending on the type of cells, 100–600 nm in diagonal length) with regard to lateral diffusion of many membrane proteins, including transferrin receptors (TR), α_2-macroglobulin receptors, epidermal growth factor receptors, E-cadherin, and anion channel band 3 (see the model shown in Fig. 1 *A*, Kusumi et al., 1993; Sako and Kusumi, 1994; Sako and Kusumi, unpublished observations). Quantitative analysis of the trajecto-

1. *Abbreviations used in this paper*: Acc, initial acceleration; d_f, dragged distance; d_r, rebound distance; G40, 40-nm colloidal gold particle; GPI, glycosylphosphatidylinositol; L210, 210-nm latex particle; L_r, diagonal length; NRK, normal rat kidney; SPT, single particle tracking; TR, transferrin receptor.

ries of TR and α_2-macroglobulin receptor molecules in the plasma membrane of NRK cells, as observed by conjugating nanometer-sized colloidal gold particles, has indicated[2] that (*a*) the plasma membrane is compartmentalized into many small domains of ~0.25 μm^2 (at 37°C) with regard to lateral diffusion of TR and α_2-macroglobulin receptor, (*b*) Tr and α_2-macroglobulin receptor molecules move from one compartment to adjacent compartments an average of once every 29 s, (*c*) within a domain, these receptor molecules undergo rapid lateral diffusion that is indicative of free diffusion within a compartment (microscopic diffusion coefficient ~10^{-9} cm^2/s), (*d*) the rate of long-range diffusion of these receptors is determined by the size of the compartment and the frequency of jumps between compartments rather than by the microscopic diffusion rate, and (*e*) partial destruction of microfilaments or microtubules dramatically changes the motional modes of these receptors, with the destruction of microfilaments having the greater effect (Sako and Kusumi, 1994).

These results were consistent with the "membrane-skeleton fence model" we proposed previously (Tsuji and Ohnishi, 1986; Tsuji et al., 1988; Kusumi et al., 1993; Sako and Kusumi, 1994). This model proposes that the membrane-associated part of the cytoskeleton (membrane skeleton) provides a barrier to free diffusion of membrane proteins due to steric hindrance (the space between the membrane and the cytoskeleton is too small for the cytoplasmic portion of the membrane protein to pass), thus compartmentalizing the membrane into many small domains for diffusion of integral membrane proteins. The membrane proteins can escape from the domains because of the dynamic properties of the membrane skeleton: the distance between the membrane and the skeleton may fluctuate over time, thus giving the membrane proteins some probability to pass the barrier, or the membrane-skeleton network may form and break continuously due to the dissociation-association equilibrium of the cytoskeleton ("fence model," Fig. 1, *A* and *B*, *b*).

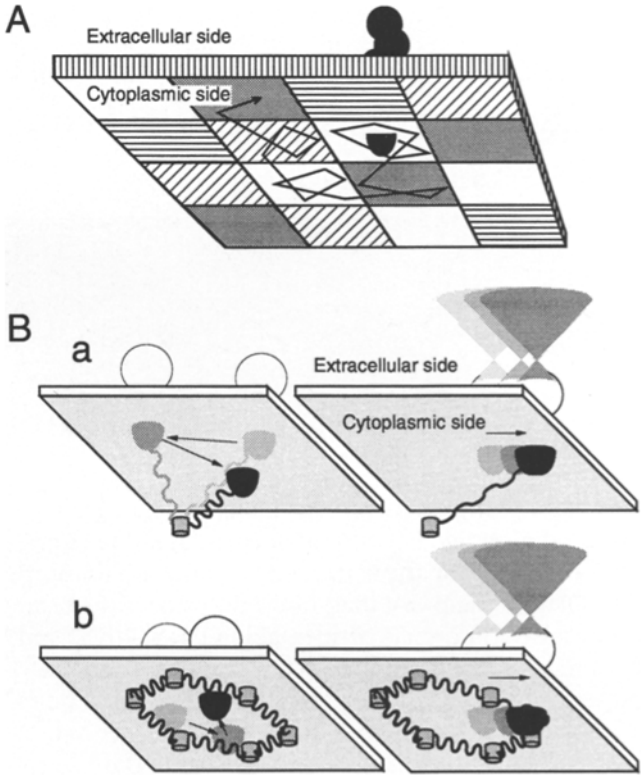

Figure 1. Schematic models of (*A*) the compartmentalized structure of the plasma membrane (membrane-skeleton fence structure) and diffusion of TR in the structure, and (*B*) the optical tweezers experiments of TR–particle complexes that are (*a*) anchored to a tethering structure and (*b*) confined by the membrane-skeleton network. (*A*) A model of the plasma membrane viewed from inside the cell. The plasma membrane is compartmentalized into many domains of ~0.3 μm^2 for diffusion of transmembrane receptor molecules. The receptor molecules undergo almost free diffusion within a domain (microscopic diffusion coefficient of ~10^{-9} cm^2/s, i.e., slowed only by the presence of other membrane proteins), to which they are confined for an average duration of ~29 s. The receptor molecules move from one compartment to adjacent domains at a frequency of ~0.034 s^{-1} (2 min^{-1}), on average, and long-range diffusion of receptors is the result of successive intercompartmental movements. Therefore, the macroscopic diffusion rate is determined from the size of the compartment and the frequency of jumps between compartments. (*B*) Two models for restriction of TR diffusion and movements forced by the laser optical trap. (*a*) Tethering model: TR is tethered or anchored to the cytoskeleton/membrane-skeleton network. (*b*) Membrane-skeleton fence model: movements of TR are limited by compartment boundaries consisting of membrane-skeleton network barriers that are attached to the membrane. See the text for details.

The first objective of the present study is to characterize the properties of the boundaries between the compartments, and to examine the membrane-skeleton fence model. Mechanical properties of the interaction between the receptor and the membrane skeleton were investigated. The force required to move the receptor past the membrane-skeleton fence, and the elastic properties of the membrane skeleton were also studied.

In addition, some fraction of the same receptor species is often anchored to the membrane skeleton or clathrin-

2. It is important to realize that classification of the motional modes into simple Brownian, directed (with a uniform drift velocity), and confined (compartmentalized) diffusion is based on statistical analysis rather than visual observation of the trajectory. See Figs. 4 and 5 in Sako and Kusumi (1994) and Figs. 4 and 6 in Kusumi et al. (1993) for quantitative statistical analysis. The statistical test for the confined diffusion within a compartment during a certain time period is based on the ratio of D_{micro} (the step size in the case of computer-generated trajectories) and the size of the compartment (whose presence is going to be tested), i.e., $4 \cdot D_{micro} \times$ (dwell time in the region) >>the compartment size. In representative cases, the trajectories of confined diffusion such as those of TR shown in Fig. 2 in Sako and Kusumi (1994) and the trajectories of simple Brownian trajectories that show apparent domains (e.g., Fig. 1.4 in Berg's book [1983]) are clear even by eye-balling this ratio. Another important feature of the trajectories of intercompartmental hop diffusion is that the adjacent compartments are almost always closely apposed to each other (see Fig. 2, *C* and *D* in Sako and Kusumi, 1994). This happens very rarely in the simple Brownian case (see Berg's trajectory). However, we would like to emphasize that these are qualitative rule of thumb, and all determination of the modes of motion must be based on quantitative statistical analysis.

A fundamental property of a fractal process is that it appears the same at all distance scales and all time scales. Our conclusion in our previous paper was that this is not true for ~80% of TR, and, therefore, TR diffusion cannot be simple Brownian diffusion. Compare Figs. 4 *C* and 8 in Sako and Kusumi (1994). The diffusion process of TR as analyzed from the perspective of the long-tail kinetics model will be discussed in the Discussion.

coated structures ("tether model," Fig. 1 *B*, *a*). In the case of TR, it has been proposed that the slowly moving component (10–20% of TR) is bound to clathrin-coated structures (Sako and Kusumi, 1994). In the case of band 3 in the human erythrocyte membrane, we found that 20% of band 3 molecules are bound to the membrane skeleton at 37°C, while movements of 80% of band 3 (mobile component) can be explained in terms of restriction by a spectrin tetramer fence (Tsuji et al., 1988). Thus, the second objective of this study is to unequivocally distinguish between the fence model and the tether model.

To address these questions, we employed a single-beam gradient force optical trap (Ashkin, 1970; Ashkin et al., 1986, 1990; Berns et al., 1989, 1991; Block et al., 1990; Edidin et al., 1991; Block, 1992; Kuo and Sheetz, 1992; Weber and Greulich, 1992; Schmidt et al., 1993; Edidin et al., 1994), also referred to as laser tweezers or optical tweezers, to move TR molecules along the plasma membrane. By using the laser trap to apply restraining forces to particles, we are able to capture, move, and release particle–TR complexes in the membrane at will. For example, Kucik et al. (1991) used laser tweezers to move particle–glycoprotein complexes to various locations on the cell surface and to restrain bead movement at specific locations in the cell. If an infrared laser is used, the intensity levels required to control particle positions produce negligible damage in living cells. Living bacteria and yeast cells have been held in a laser trap for 5 h without apparent damage, and were even observed to reproduce while trapped (Ashkin et al., 1987).

Edidin et al. (1991) moved major histocompatibility complex class I molecules that were either transmembrane-(H-2D^b) or glycosylphosphatidylinositol (GPI)-anchored (Qa2) in the plasma membrane of cultured cells. These proteins were labeled with antibody-coated gold particles and moved by laser tweezers until they escaped from the trap when they encountered barriers. Thus, the barrier-free path lengths could be obtained. At the trapping force used in their study, the barrier-free path lengths were 3.5 and 8.5 μm for transmembrane and GPI-anchored species, respectively, at 37°C. More recently, Edidin et al. (1994) measured the barrier-free path length of various mutant H-2D^b molecules which have large deletions in the cytoplasmic domain, and found that the mutant with only four amino acid residues in the cytoplasmic domain (vs. 31 residues in the wild type) exhibited the barrier-free path length about twice longer than that for the wild type. These results suggest that the cytoplasmic domain of the transmembrane protein is involved in the regulation of lateral movements of these proteins. However, these barrier-free path lengths reported previously are much greater than that one might expect from the membrane skeleton fence structure estimated from the movements of TR, which predicts the presence of barriers for laser dragging at ~300 nm on average at 37°C (half of the domain size of 620 nm, Sako and Kusumi, 1994).

In the present study, the responses of TR to a dragging force applied by the movement of a laser optical trap were quantitatively examined. TR molecules were labeled by either transferrin-conjugated 40-nm colloidal gold (G40) or 210-nm latex (L210) particles. The TR-particle complexes were moved until they escaped from the laser trap and the distances the complexes were dragged were measured at various trapping forces. The relationships between the dragged distance and both the diffusion coefficient and the confined area that the particle exhibited in the absence of the laser trap were examined to elucidate the molecular mechanisms by which the movements of TR are regulated. The mechanical properties of the compartment boundaries and the structures that anchor TR were characterized. It is concluded that the membrane-skeleton fence structure is a basic feature of the plasma membrane and that the fence structure is elastic.

Materials and Methods

Preparation of Transferrin-conjugated Small Particles

Colloidal gold particles (40-nm diam) were prepared and conjugated with bovine holo transferrin (Wako, Tokyo) as described previously (Sako and Kusumi, 1994).

L210 conjugated with transferrin were prepared by mixing 600 μl of 1 mg/ml transferrin in PBS (140 mM NaCl, 10 mM sodium phosphate buffer, pH 7.0), 40 μl suspension of L210 (Polysciences, Warrington, PA), and 810 μl of PBS. The suspension was incubated for 1 h at room temperature. A concentrated solution of BSA (10% in water, pH 7.0; Sigma, St. Louis) was added to a final concentration of 1% (wt/wt). After incubating for 1 h, the suspension was centrifuged at 8,000 *g* for 10 min. Supernatant was recovered and mixed with 6 ml of 1% BSA in PBS. The L210-transferrin complex was then washed by repeating centrifugation and resuspension two times (60,000 *g* for 20 min). The pellet was resuspended in 1.5 ml of Hanks' balanced salt solution containing 1% BSA and 5 mM piperazine-*N*,*N*′-bis(2-ethanesulfonic acid) (Pipes; Wako) (pH 7.4), filtered through a 0.22-μm membrane filter (Millipore Corp., Bedford, MA) and stored at 4°C.

Cell Cultures and Gold Labeling

An NRK fibroblast cell line was routinely cultured in a MEM (Earle's salt) supplemented with nonessential amino acids and 10% fetal bovine serum under 5% CO_2 at 37°C. Cells used for microscopic observation were cultured on 18 × 18-mm cover slips (No. 1) for 2 d after plating. The cells on a cover slip were washed with ice-cold MEM twice, cooled on ice for 10 min, and then incubated with a 60 μl suspension of ~1.5 nM particles conjugated with transferrin on ice for 45 min. After washing with MEM, preparations for microscopy were made by inverting the coverslip with the cells and a drop of MEM buffered with 5 mM Pipes (pH 7.2) on a microscope slide glass using strips of adhesive tape (~0.15 mm thick) as spacers. The medium was perfused by hand every 10 min.

Specificity of the binding of the particles to the receptor molecules was examined by incubating the cells at 4°C with ~1.5 nM particles in the presence of a 100-fold excess amount of the free ligands (both were added simultaneously). The cells were then fixed and examined by video-enhanced microscopy. As another control, binding of gold particles that were coated only with BSA to the cells was examined.

Single Particle Tracking and Laser Tweezers

The movements of L210 and G40 were observed using an instrument described by Kusumi et al. (1993). Briefly, images of the cells and the particles were obtained by video-enhanced differential interference contrast optical microscopy using an oil-immersion condenser lens (NA = 1.4; Carl Zeiss, Inc., Thornwood, NY) and an oil-immersion objective lens (100×, NA = 1.3, Plan Neofluar; Carl Zeiss, Inc.), and recorded on a laser disk recorder. The temperature of the sample was maintained at 25 ± 1°C by covering the microscope with a specially designed plastic chamber and controlling the temperature with a temperature controller (model NP-2; Nikon Inc., Instr. Corp., Melville, NY).

For optical trapping of particles, a 1063-nm laser beam from a Nd/YAG laser (model ALC D500; AmocoLaser Co., Naperville, IL, 350 mW output power [380 mW actual power]) was introduced to a microscope (Axioplan; Zeiss) through an epi-illumination light path. The laser beam was expanded to fill the aperture at the back focal plane of the objective, and then focused to form a 1-μm spot on the specimen. The maximum inci-

dent laser power just before the objective was 310 mW, and after the objective (100×; Plan Neofluar) was 100 mW. To scan the laser beam in x and y directions, two mirrors were set on scanners just before the entrance of the microscope (model 6000 and MmPIC-20A; General Scanning, Watertown, MA) which were controlled by a microcomputer.

Calibration of the Trapping Force of the Laser Tweezers

Latex and gold particles that were conjugated with transferrin were suspended in sucrose solutions of various concentrations and dragged by the optical tweezers at laser powers of 100, 50, and 25 mW (measured just after the objective lens). By varying the laser scan speed (v) or the solution viscosity (η) independently, conditions under which half of the particles were dragged for more than 20 μm were found, and the trapping force (F) under these conditions was determined using Stokes' equation, $F = 6\pi a\eta v$ (a = radius of the particle). In the present setting of the instrument, the scan speed could be varied from 0.6 to 18 μm/s under a 100× objective. The viscosity of the solution was varied from 0.89 to 43.4 × 10^{-3} Ns/m^2 (0.89–43.4 cP) by varying the sucrose concentration (the temperature was fixed at 25°C). The forces obtained by varying the scan speed and the viscosity agreed within ± 0.03 pN in all ranges of the trapping force used in this study.

Lateral Dragging of TR–Particle Complexes along the Plasma Membrane

All of the experiments were performed using cells 2 d after transfer to subculture. To reduce the internalization rate of TR, all of the experiments were performed at 25°C within 20 min after the cells were mounted.

For observation and optical trapping of each particle, movements of a target particle were initially recorded for 10 s (300 video frames). The particle was then captured and dragged by the optical tweezers. Dragging was performed by scanning the trapping laser beam at a velocity of either 0.6 or 2.4 μm/s for a distance of 2 μm, and then scanning backward to the initial position at the same speed. Scanning was repeated four times in different directions (east, north, west, and south). Finally, the trapping beam was turned off and the movements of the particle in the absence of the laser trap were recorded again for 10 s. Laser trapping was performed at three laser powers by attenuation with neutral density filters (100, 50, and 25 mW). Trajectories, diffusion coefficients, and confined areas of the particle were obtained as described by Kusumi et al. (1993).

Results

Labeling of TR with Colloidal Gold Particles on the Cell Surface

The cells were observed at 25 ± 1°C by video-enhanced differential interference contrast microscopy. A lower temperature was employed to slow internalization of particles. The number of particles located on the cell surface under these conditions was ~100/cell. These particles were scattered over the entire cell surface.

Specificity of this binding was examined by incubation with the particles in the presence of a 100-fold excess amount of the free ligands (which was premixed with the particles before addition to cells) at 4°C at which internalization of receptors does not take place. The binding of particles was inhibited to only several particles/cell (data not shown). This result suggests that the binding is specific for TR, and also suggests that the avidity effect, i.e., increases in the effective binding rate and/or the effective binding constant of transferrin due to multivalency of the beads, was small. Mecham et al. (1991) also suggested that the gold particles behave as individual ligand molecules and can be used to predict both the location and binding properties when they studied the elastin/laminin-binding protein using single particle tracking. The particles that had been coated only with BSA did not bind to the cells (a few particles/cell).

Clathrin-coated structures (coated lattices + coated pits, Miller et al., 1991) occupy ~2% of the membrane area in NRK cells, as determined by electron microscopy and by indirect immunofluorescence staining using anti clathrin antibodies (data not shown). Electron microscopy according to the method of Aggeler et al. (1983) and Miller et al. (1991) showed that ~5% of the gold particles that are attached to TR are located in coated structures in the steady state (data not shown, Takeuchi et al., 1992) However, during observation by video-enhanced microscopy, we were unable to tell which particles were actually in the coated structures. Since, under a video-enhanced contrast microscope, endosomes that showed higher contrast than usual endosomes were abundantly observed inside the cells that had been incubated with the particles, we think that most particles that were attached to the receptors did not inhibit the receptors' entry into the coated pits.

The movements of the attached particles on the surfaces of living cells were investigated. The position of each particle was determined frame by frame using the method developed by Schnapp et al. (1988). The spatial precision for determining the horizontal and vertical coordinates was 1.8 and 1.4 nm, respectively, for 40-nm gold particles fixed on a cover slip.

Majority of Transferrin Receptor Undergoes Confined Diffusion with Large Microscopic Diffusion Coefficients (≥1.5 × 10^{-10} cm^2/s) of ~10^{-9} cm^2/s on Average

TR molecules in the plasma membrane of living NRK cells were labeled with either L210 or G40 particles conjugated with transferrin.The movements of TR–G40 have been characterized previously (Sako and Kusumi, 1994). In the present study, all experiments were carried out at 25°C (37°C previously) to slow internalization of TR for experiments for longer periods of time. Approximately 90% of TR exhibited the confined diffusion mode for both L210 and G40 labels. G40- and L210-labeled TR showed similar microscopic diffusion coefficients (12.1 and 8.5 × 10^{-10} cm^2/s on average, respectively), D_{micro}, i.e., the diffusion coefficient within a compartment, which is determined from the initial slope of the plot of the mean-square displacement vs. the time interval (Table I). Histograms for the distribution of D_{micro} indicated that a higher percentage of L210 particles (22%) exhibited D_{micro} smaller than

Table I. Microscopic Diffusion Coefficient and L_r of the Confined Area for TR Complexed with L210 or G40 at 25°C

	Microscopic diffusion coefficient			L_r		
	Average ± SD	Median	n*	Average ± SD	Median	n*
	D micro, 10^{-10} cm^2/S			*nm*		
L210	8.5 ± 8.1	6.5	104	630 ± 440	480	89
G40	12.1 ± 11.5	8.6	92	820 ± 580	580	88

*n indicates the number of particles observed.
SD includes both experimental error and the true distributions. n for the area size is smaller because 5–10% of particles did not show confined-type diffusion, and also because L_r could not be determined for ~5% of particles due to large anisotrophy of the confined domain.

1.5×10^{-10} cm^2/s than G40 particles (9%) (data not shown. The reason for choosing a value of 1.5×10^{-10} cm^2/s will be clarified later).

These results suggest either that there is a greater resistance (effective viscosity) to L210 on the cell surface (than to G40) or that L210 induces TR aggregation. These data by themselves do not tell which is correct, but we think that L210-induced TR clustering is more likely based on the results of laser tweezers experiment. Since the diffusion coefficients for L210–TR are still large (compared with those for G40–TR), the aggregates should be small enough to diffuse more or less freely within a compartment in the membrane. The estimated compartment size based on the movement trajectories is 820 and 630 nm for G40 and L210 labels, respectively (Table I, also see Kusumi et al., 1993, and Sako and Kusumi, 1994 for additional theory and detailed data).

There are reports of reduced mobility of membrane proteins due to interactions on the extracellular surface of the membrane (Wier and Edidin, 1988; De Brabander et al., 1991; Sheetz, 1993). Therefore, it is possible that movements of TR are reduced by interaction between the extracellular matrix and the attached particles, with the extent of reduction being larger for L210 than for G40. In fact, Lee et al. (1993) have shown that the effective viscosity of the pericellular matrix can be as large as 0.5–0.9 poise as observed with 30-nm-ϕ gold particles attached to the headgroup of a phospholipid. However, since the difference in D_{micro} between L210 and G40 is much smaller than that expected based on the reduction by viscosity (a factor of ~5), the influence of effective viscosity on the particles on the extracellular surface is not believed to be a major rate-determining factor in the present experiments.

Dragging of TR in the Plasma Membrane

The particles bound to TR molecules were captured by optical tweezers and the particle–TR complexes were moved laterally along the plasma membrane by scanning the trapping laser beam in four directions (north, south, east, and west). The trapping force depends on the laser power and the particle properties: 0.8, 0.35, and 0.1 pN for L210 and 0.25, 0.1, and 0.05 pN for G40 at incident laser powers of 100, 50, and 25 mW, respectively, which were measured just after the beam exited from the objective lens. Note that the trapping force was calibrated with particles coated with transferrin (see Materials and Methods). As long as the force exerted on TR by the membrane or other cellular structures (such as the cytoskeleton/membrane-skeleton and clathrin-coated structures) was less than the maximal force of the trap, particles dragged along the plane of the membrane remained within the trap. The laser beam was moved a distance of 2 μm (forward and then backward, making a round trip) along the membrane plane in each direction at velocities of 0.6 or 2.4 μm/s. Particles for the dragging experiments were selected from the entire cell surface, and we did not observe any systematic difference that depends on the location within a cell. The cells and the particles were visualized by video-enhanced contrast differential interference contrast microscopy (Fig. 2 *A*) and the movements of particles were analyzed with nanometer-level spatial precision and 33 ms temporal resolution (Kusumi et al., 1993). In Fig. 2 *B*, typical examples of displacement, velocity, and acceleration of a particle induced by the movement of the optical trap (the scan of the trapping laser beam) are shown as a function of experiment time. The large variation in the velocity at ~1/3 of

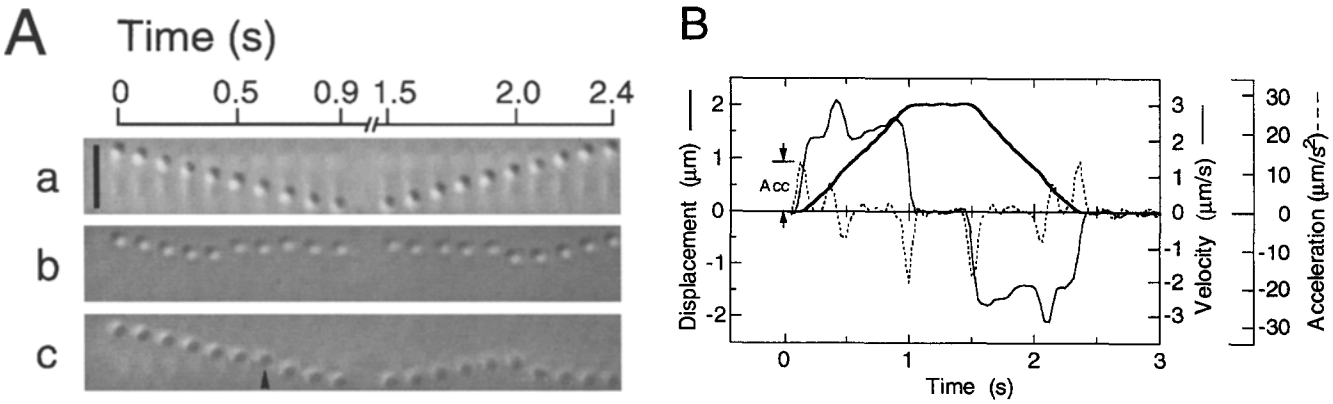

Figure 2. Dragging of cell surface TR labeled with latex beads (L210) using laser tweezers. The receptor-L210 complexes were dragged by moving the laser beam of the optical tweezers. The beam was moved 2 μm on the cell surface at a velocity of 2.4 μm/s, and was then moved backward to the starting position (down and then up). Trapping laser power in these images was 100 mW, measured immediately after the objective lens, which provides a trapping force of 0.8 pN for L210. (*A*) Serial microscopic images of particles which were dragged by the laser tweezers. Images of the particles were obtained by video-enhanced differential interference contrast microscopy. (*a*) A particle which was dragged all the way (2 μm) and then back to the starting position. (*b*) A particle that escaped from the optical trap during the forward scan. The particle escaped ~0.4 s after starting the scan, and rapidly moved back toward the starting position (by 0.5 s). At ~2.0 s, it was trapped again by the returning beam. (*c*) A particle that escaped during the backward scan of the laser trap. This particle was dragged to the end of the forward scan (2 μm away from the initial position), and escaped at ~2.0 s in the return portion of the trip. The particle showed retardation in the forward scan (arrow head) near the position at which it escaped in the backward scan. Bar, 2 μm. (*B*) A typical dragging pattern of a particle shown as a function of time. Displacement (*thick solid line*), velocity (*thin solid line*), and acceleration (*broken line*) are shown as functions of time. These parameters were obtained every 33 ms (video frame rate) and averaged over three successive points. Acc (initial acceleration) is defined as shown. A large variation in the velocity display at ~0.4 s (near the 1/3 point) in the forward scan is probably not due to Brownian motion because a similar variation is seen at 2.1 s (near the 2/3 point) in the backward scan.

Table II. d_f and Acc for the Slow Component (i.e., the Particles with $D_{micro} < 1.5 \times 10^{-10}$ cm²/s)

Particles	Trapping power		% Escaped cases	Dragged distance*	Initial acceleration*
	mW	*force, pN*	*d < 1.8 μm*	*nm*	*μm/s²*
L210	100	(0.8)	95 (39)§	240 ± 220	15 ± 8.8
L210	50	(0.35)	100 (18)	120 ± 180	9.7 ± 11.0
L210	25	(0.1)	100 (28)	47 ± 66	7.5 ± 8.4
G40‡	100	(0.25)	95 (20)	190 ± 150	15 ± 8.2

*Mean ± SD. SD includes both experimental error and the true distributions.
‡Data for G40 under other trapping forces are not listed due to the small number of the slow component observed.
§Numbers in parentheses in this column indicate the actual number of cases observed.

the forward trip is probably not due to thermal fluctuation of the particle's movement because a similar variation is observed in the backward scan. We speculate that these variations (around the peaks in the velocity display) reflect the passage of the TR over an obstacle in the dragging path because similar variations are present in both the forward and backward scans.

Trajectories of the Dragged TR Suggest the Presence of Barriers in the Dragging Path

The movements of TR molecules as they are moved by the laser tweezers at different trapping forces are shown in Fig. 3. At a trapping force of 0.8 pN, majority (67%) of the

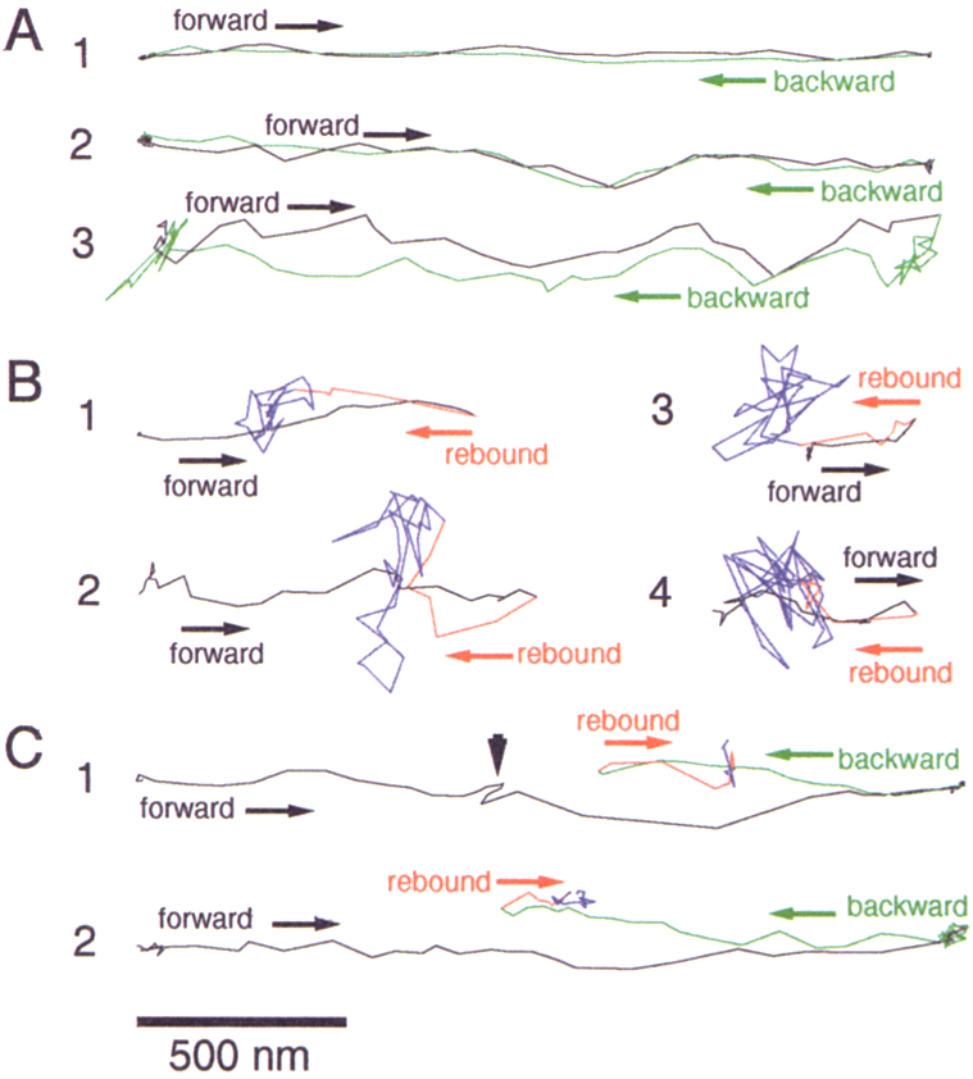

Figure 3. Trajectories of TR–particle complexes, showing dragging by and escape from the laser trap. To produce these trajectories, the x and y coordinates of the particles were determined frame by frame, and then simply connected by straight lines. The accuracy of coordinate determination has been shown to be better than 1.8 nm for particles fixed on the cover glass (Kusumi et al., 1993). Arrows indicate the direction of the laser trap scan. In the presentation of trajectories in this figure, particles are initially moved from left to right (forward scan or outbound trip), and then from right to left (backward scan or return trip). Various zones in the trajectory are shown in various colors: *black*, forward scan; *green*, backward scan; *red*, fast rebound movement for 0.2 s; *blue*, Brownian movements after fast rebound motion. (*A*) Trajectories of TR–particle complexes dragged to the end of the scan. Under weaker trapping forces (*2* and *3*), the particles showed tottering within the trap. This tottering was probably not due simply to Brownian motion, but rather to obstacles in the dragging path, since the trajectories in the backward scan coincide with those in the forward scan. (*1*) L210–TR dragged at a laser power of 100 mW (trapping force of 0.8 pN). (*2*) L210–TR dragged at a laser power of 50 mW (0.35 pN). (*3*) L210–TR dragged at a laser power of 25 mW (0.1 pN). (*B*) Trajectories of particles that escaped during the forward scan. The particle–TR complexes were dragged from left to right as shown in black. After the particles escaped from the optical trap, they often rebounded very rapidly toward the initial starting position (the red portions of the trajectories, which is ~0.2 s long) and then began to exhibit Brownian diffusion (the blue portions of the trajectories). (*1* and *2*) L210 at laser powers of 100 mW (*1*, 0.8 pN) and 50 mW (*2*, 0.35 pN). (*3* and *4*) G40 at laser powers of 100 mW (*3*, 0.25 pN) and 25 mW (*4*, 0.05 pN). (*C*) Trajectories of particles that escaped during the backward scan (the green portions of the trajectories). After the particles escaped from the optical trap, they often moved backward (in the direction of the turn-point, shown in red for ~0.2 s) and began to exhibit Brownian diffusion (*blue*). Near the position where the particle escaped, a deviation is often found in the forward trajectory (a vertical arrowhead in trajectory 1), which suggests that the particle hit the same boundary or obstacle in both directions. (*1*) L210 at 100 mW (0.8 pN). (*2*) G40 at 25 mW (0.05 pN). Bar, 500 nm.

Table III. d_f for the Fast Component (i.e., the Particles with $D_{micro} > 1.5 \times 10^{-10}$ cm²/s) of TR–L210 and TR–G40

	Trapping power		Percentage of escaped cases	d_f*
	mW	*force, pN*	$d_f < 1.8\mu m$	*nm*
TR–L210	100	(0.8)	33 (19)‡	460 ± 380
	50	(0.35)	71 (82)	640 ± 500
	25	(0.1)	72 (77)	510 ± 400
TR–G40	100	(0.25)	8 (3)‡	660 ± 380
	50	(0.1)	52 (56)	580 ± 510
	25	(0.05)	60 (57)	400 ± 430

Particles that were dragged to the end of the scan are not counted in this table.
*The average d_f for the particles that escaped during the forward scan (particles that were dragged to the end of the scan are not counted here). Mean ± SD. SD includes both experimental error and the true distributions.
‡Numbers in parentheses in this column indicate the actual number of cases observed.

TR–L210 complexes that showed fast lateral diffusion ($D_{micro} > 1.5 \times 10^{-10}$ cm²/s) were moved to the maximum extent of the laser scan (2 μm) and then returned to the initial position (Fig. 3 *A*, trajectory 1, the forward trajectories are shown in black, while the return trip is shown in green, Table III).

At lower trapping forces, the particles' trajectories under laser dragging became tottery. This tottering was not solely due to Brownian motion within the laser trap, since the trajectory of the return portion of the trip often agreed fairly well with that of the forward portion (Fig. 3 *A*, trajectories 2 and 3). These results show that the trajectories are sensitive to the presence of obstacles in the dragging path.

With weaker trapping forces, particles often escaped from the tweezers during either the forward or backward trip (Fig. 3, *B* and *C*). When the particles escaped from the optical trap in the forward trip, they often rebounded very rapidly toward the initial starting position (toward left in Fig. 3 *B*, the red portions of the trajectories) for ~0.2 s, and then began to exhibit Brownian diffusion (the blue portions of the trajectories). When such fast rebound motion is viewed in the video monitor, it looks as if the particle were catapulted off (like an arrow released from a bow), which suggests that the obstacle (or boundary or fence) is an elastic structure. Such movement, however, cannot be hurled motion of the particle. Since viscosity rather than inertia is dominant for determining the movements of submicrometer objects, the particles would stop as soon as they are released from the elastic boundary. Therefore, such fast rebound motion of the particles is likely to reflect the motion of the elastic boundaries that are restoring their original shapes.

Fig. 3 *C* shows the trajectories of particles that escaped during the backward scan (the green portions of the trajectories). After the particles escaped from the optical trap, they often moved backward (in the direction of the turnpoint, shown in red for ~0.2 s) and began to exhibit Brownian diffusion (shown in blue). In the trajectory 1, near the position where the particle escaped, a deviation is found in the forward trajectory (a vertical arrowhead in trajectory 1), which suggests that the particle hit the same boundary or obstacle in both directions.

Escape during the backward trip is of particular interest because it can be readily explained by the "fence model" (Fig. 1, *A* and *B*, *b*) but not by the "tether model" (Fig. 1 *B*, *a*). Approximately 6% of the particles that were dragged to the end of the forward trip escaped during the return trip. In addition, a deviation (small rebound) was often found in the forward trajectory near the position where the particle escaped in the backward trip (Fig. 3 *C*, trajectory 1), which again suggests the presence of a barrier at the compartment boundaries (fence model rather than the tether model).

Two populations of TR Exist: One Is the Slowly Moving Fraction, Which Can Be Dragged Only Slightly, and the Other Is the Rapidly Moving Fraction, which Can Be Dragged Far

The dragged distance (d_f) of each particle was measured from the video sequence at various trapping forces. d_f is defined as the distance from the initial position to the farthest point reached by the particle in the forward scan of the laser optical trap. The distribution of d_f is shown in Fig. 4.

Under the maximum trapping power of 100 mW (0.8 pN for L210 and 0.25 pN for G40), two major populations of particles were observed in terms of their responses to the movements of the laser trap (Fig. 4, *A* and *C*). Particles in one population could be moved to the end of the scan (d_f >1.8 μm), while those in the other population escaped from the optical trap during the forward trip.

With a decrease of the trapping laser power, more particle–TR complexes escaped from the optical trap during the forward scan (Fig. 4, *B* and *D*). Most notable is the appearance of the intermediate population peaked ~1 μm, which could be dragged but not till the end of the laser scan.

In Fig. 5, d_f obtained at the maximum trapping forces is plotted as a function of the local microscopic diffusion co-

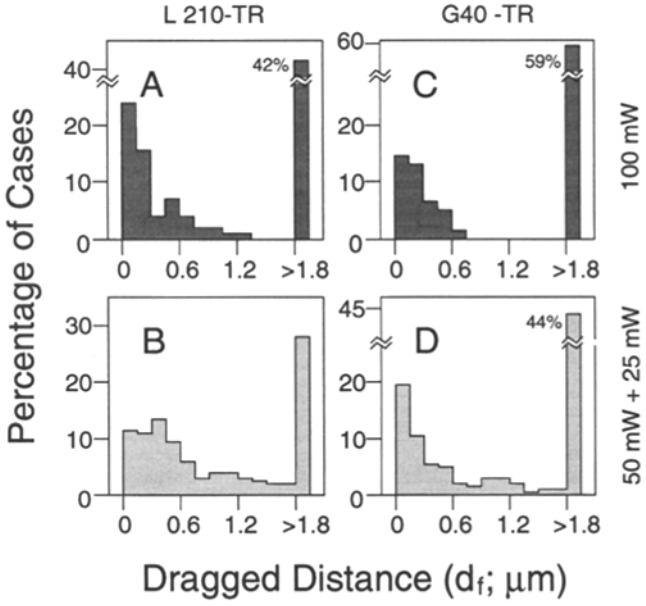

Figure 4. Histograms showing distributions of the dragged distance (d_f) of L210–TR (*A* and *B*) and G40–TR (*C* and *D*). (*A* and *C*) 100 mW of the laser power. (*B* and *D*) Combined data for the laser powers of 50 and 25 mW. The numbers of experiments carried out are (*A*) 99, (*B*) 268, (*C*) 61, and (*D*) 159.

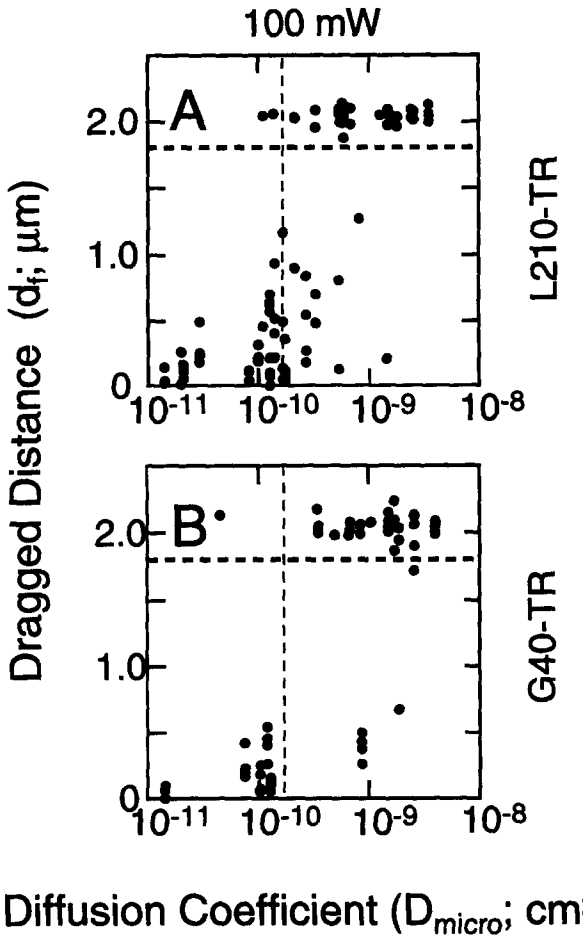

Figure 5. Dragged distance plotted against the microscopic diffusion coefficient, demonstrating a good correlation between the slow component of TR ($D_{micro} < 1.5 \times 10^{-10}$ cm²/s) and the TR population that can be hardly dragged in the dragging experiment at 100 mW, and between the fast component of TR ($D_{micro} > 1.5 \times 10^{-10}$ cm²/s) and the TR population that can be dragged till the end of the drag by a 100 mW laser trap. (*A*) L210–TR complexes. (*B*) G40–TR complexes. The vertical broken lines indicate D_{micro} of 1.5×10^{-10} cm²/s. The horizontal broken lines indicate d_f of 1.8 μm. Since the distance of the laser scan was 2 μm, the particles that can be dragged more than 1.8 μm are clustered around 2 μm. (If a longer dragging distance had been employed, many of these particles would have been moved farther.)

efficient, D_{micro}, of the individual particle. In the case of confined diffusion in a compartment, D_{micro} represents diffusion coefficient within the compartment. Both D_{micro} and the compartment size (the diagonal length, L_r) were measured both before and after the dragging experiment and the average of the two was taken. Generally, the two measurements before and after the dragging experiment gave similar values, suggesting that neither laser irradiation nor the forced movements appreciably affected diffusion characteristics of TR.

Fig. 5 shows clear correlation between D_{micro} and the dragged distance. The particles that exhibited D_{micro} greater than 1.5×10^{-10} cm²/s, which are referred to as the fast component in this paper, tended to show d_f greater than 1.8 μm, while the particles that exhibited D_{micro} smaller than 1.5×10^{-10} cm²/s, which are referred to as the slow component in this paper, generally showed d_f smaller than 1 μm (average value of d_f = 240 ± 220 nm) in the case of L210–TR, and d_f smaller than 600 nm (average value of d_f = 190 ± 150 nm) in the case of G40–TR. The separation point of the fast and slow populations, i.e., $D_{micro} = 1.5 \times 10^{-10}$ cm²/s, is shown by a vertical line in each figure in Fig. 5. (Note that the definitions of the "slow component" and the "fast component" are based on D_{micro} and not d_f). Although some particles are in the transition zone of these two populations (near the vertical line), the slow component's and the fast component's particles are generally immobile ($d_f < 300$ nm) and mobile ($d_f > 1.8$ μm) particles, respectively, in laser tweezers' experiments at 100 mW (the maximal trapping power in the present experimental setting).

In our previous paper on the movement of TR, which was studied by single particle tracking using G40, the histogram of the microscopic diffusion coefficient (D_{micro}) of the individual particle showed the presence of two populations (Fig. 6 in Sako and Kusumi, 1994): 72% of G40–TR belonged to the fast component, which represents TR with $D_{micro} > 1.5 \times 10^{-10}$ cm²/s, and 28% belonged to the slow component, which represents TR with $D_{micro} < 1.5 \times 10^{-10}$ cm²/s. Fig. 4 *C* indicate that ~30% of G40-TR exhibited d_f less than 300 nm (even at 100 mW), which is close to the percentage of the slow component (28%).

Dragging the Fast Population's TR Has Revealed the Presence of Intercompartmental Barriers (Fence Model)

Fig. 6 shows models for the interaction of TR and the intercompartmental barriers, in which the expected behaviors of TR–particle complexes that belong to the fast component are shown when they are dragged in the membrane. Fig. 6 *A* shows TR that is undergoing a rapid diffusion within a compartment of size L_r.

Fig. 6 *B* shows the behaviors of TR–particle complexes when they are dragged by a very weak optical trap. If the optical trap is sufficiently weak, the particle escapes from the trap when the particle hits the boundary first time. If we assume that the particle always escapes at the first encounter with the compartment boundary, the average d_f

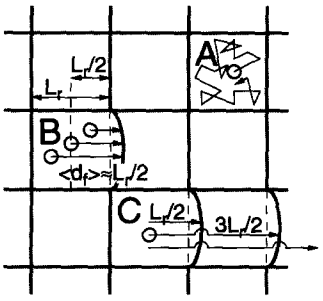

Figure 6. Models showing the behavior of particles and the membrane skeleton when the particle–TR complexes that belong to fast component are dragged in the membrane. (*A*) TR is undergoing a rapid diffusion within a compartment of size L_r. (*B*) The particle–TR complex is dragged by the optical trap. If the optical trap is sufficiently weak, the particle escapes from the trap when the particle hits the boundary first time. If we assume that the particle always escapes at the first encounter with the compartment boundary, the average d_f is $L_r/2$ because the average position of trapping (the average start point of dragging) is the center of the domain. (*C*) The fast component tends to escape from the optical trap as the particle encounters the compartment boundaries. Therefore, the distribution of d_f is likely to show peaks at $\sim L_r/2$ (350 nm), $3L_r/2$ (1 μm), etc.

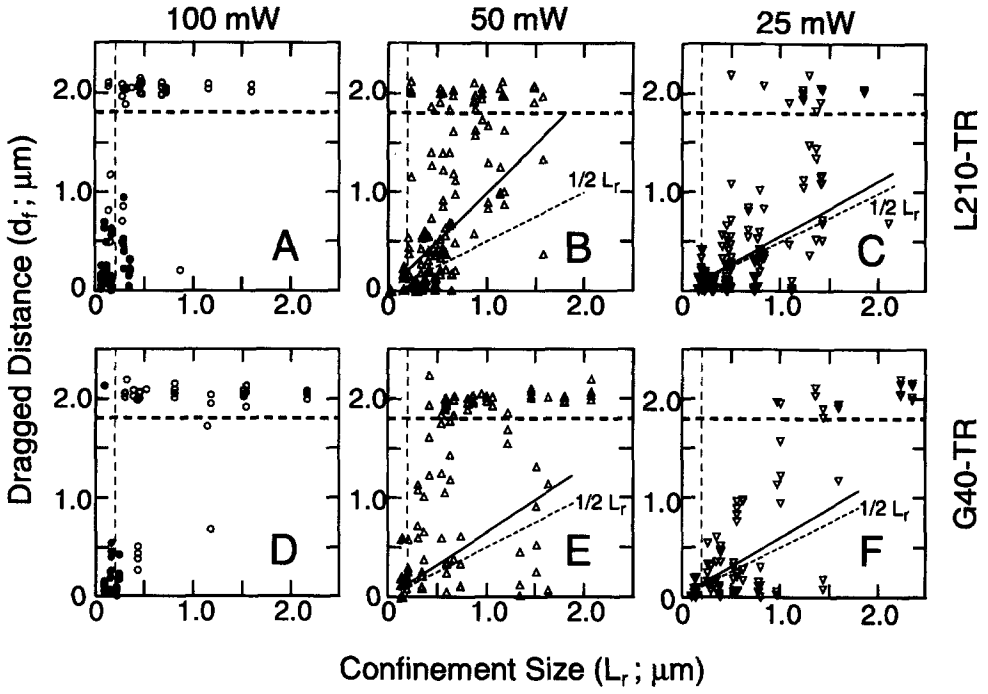

Figure 7. Dragged distance (d_f) plotted against confinement size (L_r), revealing its strong dependence on L_r. At the highest laser power (100 mW), TR showed two distinct behaviors (*A* and *D*). Both L210 (*A*) and G40 (*D*) indicate that particles with L_r smaller than ~200 nm can be dragged for short distances, while most of the particles with L_r greater than ~400 nm can be dragged to the end of the laser scan. (There is a transition zone between these populations between 200 and 400 nm of L_r). At lower laser intensities, even the particles with L_r greater than 200 nm tended to escape during the forward scan, with d_f decreasing as the laser power was decreased (*B*, *C*, *E*, and *F*). The first order correlation between d_f and L_r was determined for particles plotted in the region of $0 < d_f < 1.8$ μm and $0.2 < L_r$ (<2.5 μm), and is shown in solid lines. The regression slope determined for L210 is 0.56 (± 0.040, standard error) at a laser power of 25 mW (0.1 pN) (*C*). For G40, this value is 0.59 (±0.082, standard error) at 25 mW (0.05 pN) (*F*). If the particles always escape from the laser trap when they encounter the first boundary, the slope should be 1/2 (as shown by a broken line of $d_f = 1/2\ L_r$, see Fig. 7 *B*). The horizontal broken lines indicate d_f of 1.8 μm. Since the distance of the laser scan was 2 μm, the particles that can be dragged more than 1.8 μm are clustered around 2 μm. (If a longer dragging distance had been employed, many of these particles would have been moved farther.) The particles belonging to the fast and slow components are shown in open and closed keys, respectively. (○, ●) 100 mW; (△, ▲) 50 mW; (▽, ▼), 25 mW.

will be $L_r/2$ because the average position of trapping (the average start point of dragging) is the center of the domain.

Fig. 6 *C* shows a model in which the TR–particle complexes that belong to the fast component are dragged with a moderately strong optical trap or a strong optical trap. Escape of the TR–particle complexes from the trap takes place at the intercompartmental boundaries as the complexes encounter the compartment boundaries if they escape from the trap at all. Therefore, the distribution of d_f is likely to show peaks at $\sim L_r/2$ (350 nm), $3L_r/2$ (1 μm), etc., corresponding to the first, second encounters, etc. with the intercompartmental boundaries, respectively. With a strong optical trap, the complexes that belong to the fast component tend to stay trapped till the end of the forward trip of the optical trap.

We carried out experiments shown in Fig. 6, *B* and *C* as described below. The results agree well with the models described here, indicating that the plasma membrane is compartmentalized for the translational diffusion of TR.

The Relation between the Dragged Distance and the Confined Area (Compartment Size) Is $<d_f> = 1/2 <L_r>$ for the Fast Component, Supporting the Membrane Skeleton Fence Model

Relationships between the size of the compartment indicated by the trajectory of an individual particle (without optical trapping, L_r, for details see Kusumi et al., 1993 and Sako and Kusumi, 1994) and d_f for the same particle dragged in the optical tweezers experiments were investigated (Fig. 7).

With the highest laser power used in this study (100 mW), two major characteristic populations were found (Fig. 7, *A* and *D*), similar to the situation found in the relationship between d_f and D_{micro} (Fig. 5). One population of particles exhibited L_r smaller than 200 nm and could only be dragged for very short distances (median value of d_f ~250 nm for L210 and 220 nm for G40). The other population of particles exhibited L_r greater than 400 nm and could be dragged to the end of the forward scan ($d_f > 1.8$ μm). There are also particles in the transition zone where these two populations coexist, which is between 200 and 400 nm in L_r.

At 100 mW of the laser power, particles with L_r smaller than 200 nm (left region of the vertical broken lines in Fig. 7, *A* and *D*) could be moved to the end of the laser scan in only 2 out of 30 dragging experiments with L210, and in only 1 out of 13 experiments with G40. In fact, most particles which showed L_r smaller than 200 nm belonged to the slow component (73 and 86% for L210 and G40, respectively), suggesting that most particles with L_r smaller than 200 nm are bound to the membrane-skeleton/cytoskeleton or to clathrin-coated structures.

On the other hand, when particles showed L_r greater than 400 nm, practically all particles were dragged to the end of the forward scan ($d_f > 1.8$ μm) at 100 mW (Fig. 7, *A* and *D*).

Table IV. Regression Slopes for the Relationship between d_f and L_r for the Fast Component (the Particles with D_{micro} $>1.5 \times 10^{-10}$ cm²/s, $d_f < 1.8$ μm, no Restriction on L_r) and the Particles with $L_r > 200$ nm, as Shown in Fig. 6

Particles	Trapping power	Fast component	Particles with L_r >200 nm
	mw		
L210	50	1.0 ± 0.070	0.99 ± 0.070
L210	25	0.60 ± 0.040	.56 ± 0.040
G40	50	0.66 ± 0.11	0.66 ± 0.11
G40	25	.59 ± 0.080	.59 ± 0.082

When the incident laser power was attenuated to 50 or 25 mW, such particles with L_r greater than 200 nm began to escape from the laser trap during the forward scan (Fig. 7, *B*, *C*, *E*, and *F* in the right bottom regions). At an incident laser power of 25 mW, ~60% of G40 and 80% of L210 that exhibited L_r greater than 200 nm escaped from the laser trap during its forward scan.

In Fig. 7, *B*, *C*, *E*, and *F*, correlations between d_f and L_r at various laser powers were evaluated in the region where $L_r > 200$ nm and $0 < d_f < 1.8$ μm (*right bottom region*). Correlation estimated using Spearman's correlation coefficient by ranks indicated from medium (for G40, $P < 0.02$) to high (for L210, $P < 0.001$) correlations of d_f and L_r at 25 mW. The regression slope determined for L210 exhibiting $L_r > 200$ nm and $d_f < 1.8$ μm is 0.56 (±0.040, standard error) at a laser power of 25 mW (0.1 pN) (Fig. 7 *C*, Table IV). For G40, this value is 0.59 (±0.082, standard error) at 25 mW (0.05 pN) (Fig. 7 *F*, Table IV).

If the particles always escape at the compartment boundaries, the regression slope should be 0.5 (the average value of $d_f = L_r/2$, since the average initial position of dragging is the center of the compartment, see Fig. 6 *B*). Therefore, the close values (to 0.5) of the regression slopes obtained at 25 mW suggest that the particles tend to escape from a weak trap (0.05–0.1 pN) at the domain boundaries, if they escape at all.

The slopes obtained from the regression lines in Fig. 7 may be overestimated because some particles may escape at the second or third encounter with the boundaries (see Figs. 6 *C* and 8): even if a particle passed the first boundary, it may escape from the laser trap at the second boundary it encounters, which would be located an average of ~1 μm away from the starting point (see Fig. 6 *C*). This explanation is consistent with the observation in Fig. 7, *B* and *E*, showing that the regression slopes at 50 mW are larger than those at 25 mW (Table IV).

In the linear regression analysis between d_f and L_r at laser powers of 50 nd 25 mW above, only particles with L_r >200 nm were considered. Another logical way of evaluating the correlation between d_f and L_r is to preselect particles that belong to the fast component ($D_{micro} > 1.5 \times 10^{-10}$ cm²/s) for regression. In Fig. 7, particles belonging to the fast and slow components are shown in open and closed keys, respectively. The regression slopes obtained for the fast component (with no restriction on L_r but with a condition of $d_f < 1.8$ μm) are almost the same as those obtained for particles with $L_r > 200$ nm as listed in Table IV, and, therefore, the regression lines estimated with these two methods coincide in Fig. 7.

TR of the Slow Component Is Anchored to Elastic Structures

In the histograms shown in Fig. 4, the distributions of the dragged distance d_f for the total population of TR–particle complexes are shown. In Fig. 8, the distributions of d_f are shown separately for the fast and slow TR components (readers are requested to be careful about the definitions of the slow and the fast components. These components are defined on the basis of D_{micro} and not d_f in the present paper). Almost all of the particles with low diffusion coefficients (hatched bars in Fig. 8) escaped from the tweezers during the initial stages of forward dragging even under the maximum trapping power of 100 mW (hatched columns in Fig. 8 *A*, *a* and *d*). In contrast, large proportions of the fast component (67% for TR-L210 and 92% for TR–

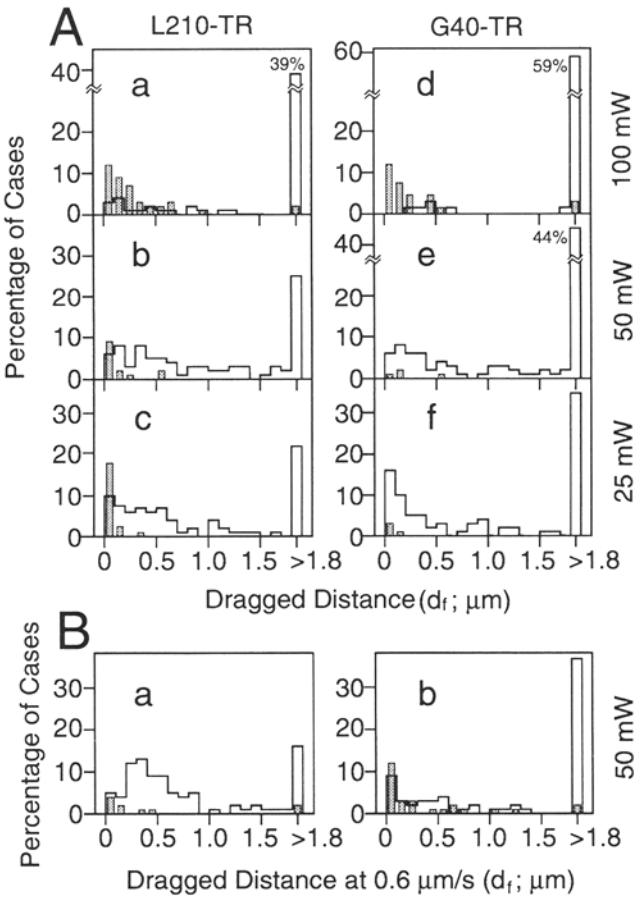

Figure 8. Histograms showing distributions of the d_f for the slow (*hatched columns*) and fast (*open columns*) components of TR. Both the laser intensity and the scan velocity of the laser trap were varied (*A*, 2.4 μm/s; *B*, 0.6 μm/s). Open column: particles with $D_{micro} > 1.5 \times 10^{-10}$ cm²/s (fast component). Hatched column: particles with $D_{micro} < 1.5 \times 10^{-10}$ cm²/s (slow component). (*A*, *a–c*) L210–TR complexes at trapping laser powers of 100 mW (*a*, 0.8 pN, 99 cases), 50 mW (*b*, 0.35 pN, 133 cases), and 25 mW (*c*, 0.1 pN, 135 cases). (*d–f*) G40–TR complexes at trapping laser powers of 100 mW (*d*, 0.25 pN, 61 cases), 50 mW (*e*, 0.1 pN, 77 cases), and 25 mW (*f*, 0.05 pN, 82 cases). (*B*) The effect of the scan speed of the laser trap. The scan speed was reduced to 0.6 μm/s and an incident laser power of 50 mW was employed. (*a*) L210–TR (0.35 pN, 101 cases). (*b*) G40–TR (0.1 pN, 89 cases).

G40, Table III) could be moved to the end of the drag (open columns in Fig. 6 *A*, *a* and *d*).

The dragged distances for the slow component (which are mostly less than 300 nm, Fig. 8 *A*) strongly depended on the trapping force. As summarized in Table II, with a decrease in the laser power for trapping, the dragged distance of the slow component decreased (also see hatched columns in Fig. 8 *A*, *a–c*). This result indicates that the force exerted on the slow component of TR, which eventually pulls TR out of the laser trap, increases as the distance from the initial location increases, suggesting that TR molecules undergoing slow diffusion are anchored to a spring-like structure, possibly the membrane skeleton/cytoskeleton or clathrin-coated structures.

The effect of the scan rate was examined by reducing it to 0.6 μm/s for a laser power of 50 mW (Fig. 8 *B*). This change did not affect the results.

TR of the Fast Component Sometimes Escapes from the Optical Trap as It Encounters the Intercompartmental Boundaries, When TR Is Dragged by a Moderately Strong Trap of 0.05–0.1 pN

The responses of the fast TR component were completely different from those of the slow component (Fig. 8). At the highest laser power used in this work (100 mW), ~70–90% of the particles that belonged to the fast component were dragged to the end of the scan (2 μm, Table III and Fig. 6 *A*, *a* and *d*).

As the trapping force was decreased, more particles escaped during the forward scan. The distributions of d_f under lower trapping forces are shown in Fig. 8 *A*, *b*, *c*, *e*, and *f* (*open bars*). Under reducing trapping forces, there are apparently three peaks in the distributions of d_f: ~300 (0–600) nm, 1,000 (700–1500) nm, and over 1.8 μm, although the central peak is rather small (also refer to Fig. 4, *B* and *D*). The peak located over 1.8 μm is an artificial one, and indicates the collective percentage of particles that were dragged over 1.8 μm. The peak centered around 300 nm shows broad distributions of d_f in this range (Fig. 8 *A*, *b*, *c*, *e*, and *f*, and *B*, *open bars*).

The average size of the compartment is ~700 nm for TR labeled with L210 or G40 (Table I). If we assume a membrane-skeleton fence model, the expected average distance to hit the fence (or the compartment boundary) the first time must be ~350 nm (700/2 nm, since the average starting point of the dragging is the center of the compartment), while that for the second time must be ~1,000 (350 + 700) nm (see Fig. 6, *B* and *C*). Therefore, the results shown in Fig. 8, particularly the presence of the two peaks at ~300 and 1,000 nm, are consistent with the compartmentalized structure of the plasma membrane for translational diffusion of TR.

The average d_f for the particles that escaped during the forward scan (particles that were dragged to the end of the scan are not counted here) was ~500 nm, and this value depended slightly on the trapping force (Table III). The slight dependence of the average d_f for the fast component on the trapping power may be due to the difference in the percentages of the population in the two peaks at ~300 and 1,000 nm (Fig. 8): at lower trapping forces, the particle–TR complex may escape from the trap more easily at its first encounter with the intercompartmental barrier. Such weak dependence on the trapping force should be contrasted to the strong force dependence of the slow component summarized in Table II. The force acts on dragged TR only when the TR molecule hits obstacles or barriers located at about 300 nm and 1 μm away (on average) from the starting point.

At the trapping power of 25 and 50 mW, the TR–particle complexes of the fast component that exhibited d_f smaller than 1.8 μm more often escaped at the first barrier than at the second barrier (Figs. 4, *B* and *D*, and 8 *A*, *b*, *c*, *e*, and *f*). Therefore, we think that, in the relationship between d_f and L_r shown in Fig. 7, *B*, *C*, *E*, and *F*, the regression slopes are near 0.5 but greater than 0.5 (also see Table IV).

Difference between G40-TR and L210-TR in their Responses to Dragging Forces

The results obtained for L210 and G40 are not consistent in terms of the trapping forces. For example, the behavior of L210 under a restraining force of 0.35 pN (50 mW, Fig. 8 *A*, *b*) is similar to that of G40 under a restraining force of 0.1 pN (50 mW, Fig. 8 *A*, *e*). If the results of L210 under 0.35 pN and those of G40 under 0.1 pN are compared, the distributions of dragged distances Fig. 8 *A*, *b* and *e*) are similar. (D_{micro} and the compartment size [Table I] are similar, as described before). The percentage of particles that escape during the forward scan of the trap tends to be larger for L210 than for G40 (Table III). These results suggest that L210 induces aggregation of TR, thereby increasing the force required to pull L210–TR past the fence. Although it would be more difficult for clusters of TR to pass the membrane skeleton fence (or to break off from the tether) than dimers (TR is an S-S linked homo dimer of 90-kD polypeptides), the effect of a small degree of aggregation on the diffusion coefficients must be small (Saffman and Delbrück, 1975). Aggregation of TR could also increase the probability of binding to the membrane skeleton, which would lend to a decrease in the diffusion coefficient, as was observed in single particle tracking experiments.

This difference between L210 and G40 in the trapping force required to pass the diffusion barriers is not likely to be linked to the difference in viscosity-induced drag on the particles (which must be ~5 times larger for L210), since similar results were obtained at the reduced rate of 0.6 μm/s (4 times smaller than in standard experiments, which will decrease the drag by a factor of 4, Fig. 8 *B*). If the difference between L210 and G40 were caused by the effective viscosity in the external periphery of the cell surface, the effect of the dragging speed would be much larger. Taken together, these results suggest that L210 induced more aggregation of TR than G40.

Half of TR-G40 Complexes of the Fast Component Pass the Boundaries When the Complexes Are Dragged at ~0.1 pN of Force

The trapping force needed to pull the particle–TR complex past the fence can be estimated for the particles with L_r greater than 200 nm or for those that belong to the fast

Table V. Acc of TR–L210 and TR–G40 at an Incident Laser Power of 100 mW (0.8 and 0.25 pN, Respectively)

Classification at $D_{micro} = 1.5 \times 10^{-10}$ cm²/s*	TR–L210		TR–G40	
	Slow	Fast	Slow	Fast
Particles escaped	15 ± 8.8 (39)	22 ± 9.1 (19)	15 ± 8.2 (20)	29 ± 3.0 (3)
Particles moved to the end (d_f > 1.8 μm)	ND	28 ± 3.6 (39)	ND	33 ± 14 (34)

Mean ± SD (number of cases). SD includes both experimental error and the true distributions.
ND, not determined because less than three cases were observed.
*The particles that have D_{micro} greater or smaller than 1.5×10^{-10} cm²/s were defined as fast and slow components, respectively.

component (Figs. 7 and 8, Table III). In both estimates, half of L210–TR and G40–TR got over the fence at trapping forces of about 0.6 and 0.1 pN, respectively. Even with weaker trapping forces (Fig. 7 *A*, *c* and *f*), some particles were able to pass the fence although the probability of passing is lower, suggesting that the energy required for passing is quite close to the thermal energy, kT (which makes passing a statistical phenomenon). In addition, the boundaries may be fluctuating or undergoing polymerization–depolymerization process continually, which enhances passing of TR over the boundaries. Of course there is always a possibility that these particles were in a compartment with L_r greater than 2 μm.

Initial Acceleration of TR Particles in Dragging Experiments Shows that TR that Cannot Be Dragged Far Is Bound to Cellular Structures

To characterize the restraining force exerted by the cell against the dragging force of the laser tweezers at the initial stages of dragging, the initial acceleration of particles (*Acc*) was estimated. Acc was defined as the maximum acceleration before the particle reached a constant velocity (Fig. 2 *B*). The average Acc for L210 and G40 particles in water under identical scanning conditions (2.4 μm/s at 100 mW) were 26 μm/s² for both particles, which should represent the maximum value of Acc for TR–particle complexes in the membrane. As the cellular restraining force exerted on a particle increases, Acc is expected to decrease because the particle cannot be accelerated as quickly as it could in the absence of restraining forces. Since, in most cases, Acc reached a maximum value before the particles were moved 60 nm, Acc was not limited by d_f. Acc's for the slow and fast components are summarized in Table V for the highest trapping power. Acc for the slow component is substantially smaller than that for the fast component, which suggests that the slow component TR is anchored to cellular structures.

Acc was somewhat difficult to determine with lower laser intensities due to large fluctuations of the trajectories induced by Brownian motion. Nevertheless, Acc's under low laser light intensities were determined for the slow component of L210 (Table II), and these data show that Acc decreases as the laser power decreases. This result indicates that the initial acceleration is a good parameter for evaluating the forces which act on TR, and suggests again that the slow component consists of TR anchored to cellular structures.

The relationships between Acc and d_f at an incident laser power of 100 mW are shown in Fig. 9. Acc increases with an increase in d_f until d_f reaches ~300 nm. For particles that can be dragged more than ~500 nm, Acc is fairly constant regardless of d_f and is near its maximum value of 26 μm/s². These results again indicate that TR molecules that can be moved only very short distances are anchored to cellular structures that have an elastic nature, and that TR molecules that can be moved for longer distances diffuse within a compartment more or less freely until they collide with the boundaries.

Rebound Distance: the Intercompartmental Barriers Are Elastic, with a Spring Constant of 3 pN/μm

As shown in Fig. 3, *B* and *C*, when particles escape from the laser trap, they almost always spring back rapidly in either their forward or backward trips. The rebound quickly ceases and the particle begins to exhibit Brownian diffusion in less than 0.2 s. These results suggest that compartment boundaries, as well as the tether (for the slow component), are elastic in nature. To characterize the boundaries and the anchoring structure of TR, the relationship between d_f and the rebound distance (d_r) was examined and the results are shown in Fig. 10.

For d_r, we measured the maximum distance the particle traveled from where it escaped from the laser trip within 0.2 s after escape (Fig. 10). The correlation between d_r and d_f was obtained for the slow component by performing a linear regression using an equation $dr = ad_f$. The regression slope *a* describes how elastic (resilient) the structure

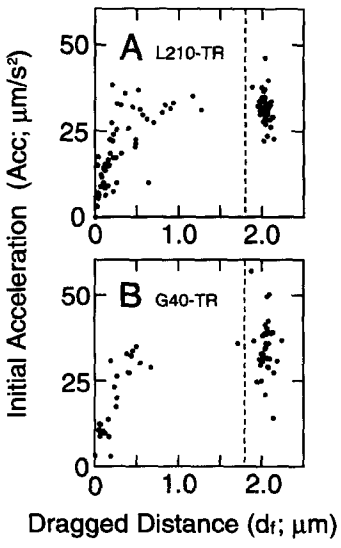

Figure 9. Initial acceleration (*Acc*) plotted against the dragged distance (d_f) under the maximum laser power (100 mW). The results suggest that the slow component is anchored to elastic cellular structures, while the fast component is not anchored. Acc is defined in Fig. 2 *B*. For particles which could be dragged only up to ~300 nm, Acc is proportional to d_f. For particles with d_f greater than 500 nm, Acc was independent of d_f. (*A*) L210-TR. (*B*) G40–TR. The vertical broken lines indicate d_f of 1.8 μm. Since the distance of the laser scan was 2 μm, the particles that can be dragged more than 1.8 μm are clustered around 2 μm.

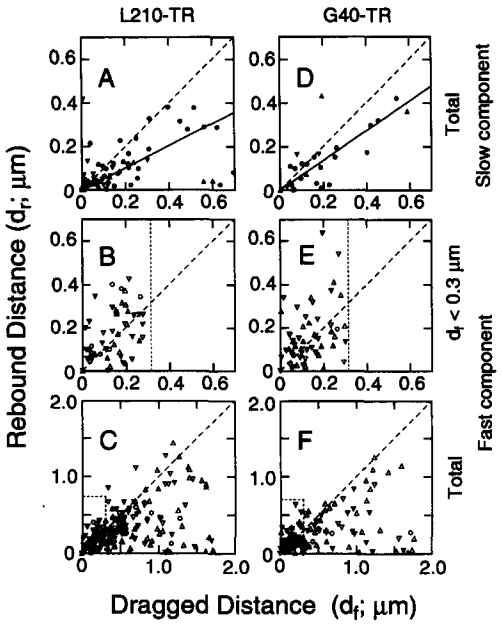

Figure 10. Rebound distance (d_r) plotted against dragged distance (d_f). (*A–C*) L210–TR. (*D–F*) G40–TR. Slow component (*A* and *D*), the fast component with $d_f < 0.3$ μm (*B* and *E*), and the total population of the fast component (*C* and *F*). In *B* and *E*, the rectangular box around the origin surrounded by the broken lines in *C* and *F* are expanded to the same scale of that in *A* and *D*, respectively. The diagonal broken lines indicate the line for $d_r = d_f$. The solid lines in *A* and *D* are the result of linear regression with a slope of 0.41 ± 0.040 (n = 84) and 0.68 ± 0.066 (n = 26), respectively. ○, 100 mW; △, 50 mW; ▽, 25 mW.

is ($0 \leq a \leq 1$) and increases as the elasticity (resilience) increases. The regression lines are shown in Fig. 10, *A* and *D* (*solid line*), and the regression slopes are 0.41 ± 0.040 (n = 84) for L210–TR and 0.68 ± 0.066 (n = 26) for G40–TR. The slow component, which we propose to represent TR that is bound to the cytoskeleton or the clathrin-coated structures, showed that these structures are moderately elastic (resilient) (Fig. 10, *A* and *D*).

Fig. 10, *B*, *C*, *E*, and *F* show the correlation of d_f and d_r for the fast component. Fig. 10, *C* and *F* shows correlation for the total population of the fast component. The rectangular region near the origin, which is surrounded by the broken lines, is expanded to the same scale as in Fig. 10, *A* and *D* (Fig. 10, *B* and *E*). Separation of the fast component into those with d_f either greater or smaller than 300 nm was done because, in addition to increasing visibility near the origin, the particles that went over the fence (at $L_r/2$ = 350 nm) and that did not (on average) should be separately discussed if we assume the membrane-skeleton fence model.

For the particles of the fast component that exhibited d_f greater than 300 nm, d_r is smaller than d_f (almost all the points are below the line of $d_r = d_f$. Fig. 10, *C* and *F*). For the particles that exhibited d_f less than 300 nm, d_r tended to be close to d_f on average (Fig. 10, *B* and *E*).

The spring constants of the boundary were estimated by both plotting force versus d_f and by plotting stress by the trapping force versus strain of the boundary (or the tether for the slow component). Since the exact shape of the force potential of the optical trap has not been determined, we made rough estimates using the maximal trapping force. The spring constant of the boundary was ~3 (±2) pN/μm, and that of the tether (to the cellular structure for the slow component) was ~12 (±8) pN/μm.

Discussion

The present results reveal the presence of two populations of TR in the plasma membrane in terms of their responses to lateral dragging forces exerted by laser tweezers at 100 mW (mobile and immobile populations). Furthermore, each of these populations exhibits distinct D_{micro} and L_r. One population represents 5–10% of TR, typically exhibits D_{micro} less than 1.5×10^{-10} cm²/s and L_r less than 200 nm, and cannot be dragged by the laser trap more than 300 nm. Acc in this population was small, indicating the presence of a force acting against the dragging. We propose that this component is bound to the cytoskeleton/membrane-skeleton and/or to the clathrin-coated lattice, as shown in Fig. 1 *B*, *a*.

The other population represents ~90% of TR, and typically exhibits D_{micro} greater than 1.5×10^{-10} cm²/s and a confinement area of 600–800 nm in diagonal length (L_r). Particles in this component can be dragged to the end of the scan of the laser trap (d_f greater than 1.8 μm for a scan distance of 2 μm) at the highest laser power, but often escape at the compartment boundaries (at $L_r/2$ and $3L_r/2$) at lower trapping forces (although the peak at ~$3L_r/2$ is slight) (see Fig. 6 *C*). Since movements of TR–particle complexes and their responses to laser tweezers are similar for both L210 and G40, and since treatment with cytochalasin D or vinblastin affects the movements of TR (Sako and Kusumi, 1994), the boundaries are likely present in the cytoplasmic domain.

Fence versus Tether

In the case of the slow component, we propose that TR is tethered to the membrane-skeleton/cytoskeleton and/or the clathrin-coated structures. Small diffusion coefficient ($D_{micro} < 1.5 \times 10^{-10}$ cm²/s), small L_r (often less than 200 nm, Fig. 7, *A* and *D*), small d_f (often less than 300 nm, Fig. 8 *A*), small Acc (Table II and Fig. 9), and the strong dependence of d_f on the trapping force (Table II) are all consistent with the tether model. An interesting observation here is that D_{micro} is still quite large compared with that for totally immobilized membrane proteins (~10^{-12} cm²/s, Kusumi et al., 1993). This result suggests that the cellular structures that TR is bound to allows TR to undergo relatively fast local movements.

For the fast component, which represents ~90% of TR, some of the results shown in this and the previous papers can be explained by both the fence and tether models equally well, if we assume that the tether is like a "loose rubber band." Since the tether is loose, the membrane proteins can undergo free diffusion until the proteins reach a point at which the tether is tight and has to be stretched for the membrane protein to move away any further. Such a model explains the confined diffusion of TR and the rebound phenomena in the forward (only forward but not backward) dragging experiments.

However, we made observations which cannot be readily explained by the loose rubber band tether model. (*a*) Some particles escaped during the return portion of the trip. Moreover, these particles usually bounced opposite the direction of the returning laser beam (toward the turnpoint, Figs. 2 *A* and 3 *C*). (*b*) The long-range trajectories we previously reported for TR and α_2-macroglobulin receptor were similar to those shown schematically in Fig. 1 *A* (Sako and Kusumi, 1994). These observations can be readily explained by the fence model, but not by the tether model. Therefore, for the fast component, we believe that the principal mechanism that restricts the movement of the fast component is confinement (fence model) rather than tethering. The cytoskeletal elements are likely to be involved in such boundaries because treatment of the cells with cytochalasin D and vinblastin strongly influenced the mode of motion (confined diffusion in particular, Sako and Kusumi, 1994).

The cytoplasmic domains of membrane proteins have been shown to be involved in controlling the lateral movements of membrane proteins in the plasma membrane for major histocompatibility complex molecules in transfected murine HEPA-OVA cells (Edidin et al., 1991), band 3 in erythrocytes, and transfected E-cadherin and its mutants in L cells. A mutant E-cadherin which has only 21 amino acid residues in the cytoplasmic domain exhibited a confinement area that was four times larger than the wild type possessing 152 residues in the cytoplasmic domain (Sako et al., 1992). Removal of the cytoplasmic portion of band 3 by trypsin (without affecting the membrane skeleton) completely freed band 3 from confinement (Tsuda et al., 1992). In addition, we have found an extensive network of membrane-skeleton/cytoskeleton composed primarily of actin filaments on the cytoplasmic surface of the plasma membrane of NRK cells (Takeuchi et al., 1992).

The compartment boundaries are elastic. Particles that escaped from the tweezers bounced elastically, and the rebound motion continued for ~0.2 s or shorter. The cytoskeletal/membrane-skeletal network has been shown to be an elastic structure in red blood cells (Waugh, 1982) and in the membrane cortex of sea urchin (Hiramoto, 1970) or various cultured cells (Bray et al., 1986). We also observed that the tether or anchoring structure for the slow TR component is elastic.

The spring constants of the boundary were estimated by both plotting force versus d_f and by plotting stress by the trapping force versus strain of the boundary (or the tether for the slow component). Since the exact shape of the force potential of the optical trap has not been determined, we made rough estimates using the maximal trapping force. The spring constant of the boundary was ~3 (±2) pN/μm, and that of the tether was ~12 (±8) pN/μm.

Compartmentalization of the Plasma Membrane and Intercompartmental Hop Diffusion of Membrane Proteins

Confined lateral diffusion of receptors has been observed in a variety of membrane proteins in various types of cells, such as TR and α_2-macroglobulin receptor in NRK cells (Sako and Kusumi, 1994), TR, EGF receptor, and E-cadherin in mouse keratinocytes (Kusumi et al., 1993), TR and transfected E-cadherin in L cells (Sako et al., 1992) and band 3 in red blood cells (Tsuda et al., 1992). Considering all of these findings, we propose that compartmentalization of the plasma membrane into numerous submicrometer domains by a membrane-skeleton/cytoskeleton meshwork (membrane-skeleton fence structure) is a basic feature of the plasma membrane. For lateral movements of individual membrane protein species, additional mechanisms that regulate movement may be at work, and these effects would be superimposed on the fence effect produced by the membrane-skeleton network. In this sense, it would be interesting to study the movements of receptors for various growth factors because a fraction of these receptors are known to bind to the cytoskeleton (Vale and Shooter, 1983; Wiegant et al., 1986; Zippel et al, 1989; den Hartigh et al., 1992).

Slowing the diffusion rate of TR in the plasma membrane may be important for its function (Gonclaves, 1993). Since TR is constantly recycled whether or not it binds to transferrin, for efficient use of energy, the resident time of TR in the plasma membrane must be sufficiently long to catch transferrin while TR is exposed to the extracellular fluid. If diffusion is fast, TR may encounter, be trapped, and internalized by the clathrin-coated pit very quickly before TR catches transferrin. The macroscopic diffusion coefficient for TR (which is smaller than the microscopic diffusion coefficient due to the presence of boundaries) is ~25 times smaller than the microscopic diffusion coefficient within the membrane compartment. De Brabander et al. (1988) followed such pathway using nanovid microscopy (single particle tracking, but without nanometer-level analysis of movements).

The mechanism that slows the movements of membrane proteins in the plasma membrane has been a long-standing problem. Lateral diffusion coefficients for most integral membrane proteins in the plasma membrane, as measured by fluorescence photobleaching recovery, are in the range of 10^{-10}–10^{-12} cm^2/s (Jacobson et al., 1987). These values are 10^2 to 10^4 times smaller than the that expected for freely diffusing proteins in lipid bilayers (Saffman and Delbrück, 1975). A variety of mechanisms have been found or proposed so far, including binding to cytoskeleton, crowding of membrane proteins in protein-rich domains (Pink, 1985; Yechiel and Edidin, 1987; Edidin and Stroynowski, 1991), the large exclusion volume of carbohydrate chains (Wier and Edidin, 1988; Lee et al., 1993), percolation diffusion due to immobile obstacles and slowly diffusing obstacles (such as proteins bound to the cytoskeleton and protein aggregates, Saxton, 1987, 1989*a*), transient binding to the cytoskeleton or to other membrane proteins bound to cytoskeleton, crowding of membrane proteins on the membrane surface (De Brabander et al., 1991; Sheetz, 1993), and the membrane-skeleton fence structure (Tsuji et al., 1986, 1988; Saxton, 1989*b*, 1990; Kusumi et al., 1993; Sako and Kusumi, 1994). The present results strongly suggest that the membrane-skeleton fence structure and binding to anchoring structures (such as coated structures and the cytoskeleton) are the major factors which regulate the movement of transmembrane proteins in the plasma membrane. Since the microscopic diffusion coefficient within the compartment is large, other mechanisms are not as important as obstruction by the

membrane-skeleton barriers in the case of TR in NRK cells.

However, we do not think that the membrane-skeleton fence is solely regulating the movements of membrane proteins. There must be many small force potentials that influence and slow the diffusion of membrane proteins, which may be due to crowding and microaggregation of membrane proteins, and due to the obstacle effect of microaggregation of membrane proteins and the membrane proteins that are bound to the membrane skeleton. These would be analyzed based on the long-tail kinetics model (Nagle, 1992). From the perspective of this theory, what we are proposing in this (and the previous) paper is that, among various molecular interaction (trapping) potentials that a diffusing TR molecule encounters in the plasma membrane, one interaction energy stands out among others, which is a corralling effect (interaction energy with the fence), possibly due to the static hindrance of the membrane skeleton. Rebound of particles after they escape from the laser tweezers, for example, cannot be explained by the long-tail kinetics model.

The wide distribution of D_{micro} of TR may be due to the presence of various mechanisms of slowing diffusion of TR in the membrane, such as those listed above, and that such local behavior of membrane proteins may be described by the long-tail kinetics. This issue is an important problem yet to be solved in the future.

We estimated that 0.6 and 0.1 pN of the trapping force is necessary to pass the boundaries for L210-TR and G40-TR, respectively. However, we do not know how long in distance this force have to be applied to TR to pass the boundary. If we assume that the width of the boundary is 6 nm and that the radius of TR is 2 nm, this distance would be 10 nm. Assuming that the average dragging force needed to pass the boundary is 0.5 pN, the work that must be done to pass the boundary is 5 pN·nm = 5×10^{-21} joule, which is only 2.5 times larger than the thermal energy, kT/2. The force potential that is corralling the membrane protein is thus just sufficient to cope with the thermal diffusion of the protein.

Biological motor proteins, such as myosin and kinesin, produce 1–10 pN of force when they decompose one molecule of ATP (Oosawa, 1977; Kishino and Yanagida, 1988; Kuo and Sheetz, 1992; Svoboda and Block, 1994; Finer et al., 1994). The displacement that decomposition of one molecule of ATP induces is apparently comparable or larger than 10 nm under a stress of 0.5 pN of external force. Therefore, the intercompartmental barriers are sufficiently low and narrow to allow the passage of TR if the cell uses biological motors and one molecule of ATP.

The function of many membrane receptors is regulated by localization, aggregation, molecular association, and assembly of the receptor, such as assembly of cadherins at the cell–cell contact sites, and of TR and other nutrition receptors at clathrin-coated structures, and oligomerization of signaling receptors, such as EGF receptors, for the subsequent cellular responses. In studies of these processes, the membrane-skeleton fence structure, binding to the membrane-skeleton, and compartmentalization of the plasma membrane must be taken into consideration.

Received for publication 17 June 1994 and in revised form 15 November 1994.

References

Aggeler, J., R. Takemura, and Z. Werb. 1983. High-resolution three-dimensional views of membrane-associated clathrin and cytoskeleton in critical-point-dried macrophages. *J. Cell Biol.* 97:1452–1458.

Anderson, C. M., G. N. Georgiou, I. E. G. Morrison, G. V. W. Stevenson, and R. J. Cherry. 1992. Tracking of cell surface receptors by fluorescence digital imaging microscopy using a charge-coupled device camera. Low-density lipoprotein and influenza virus receptor mobility at 4°C. *J. Cell Sci.* 101:415–425.

Ashkin, A. 1970. Acceleration and trapping of particles by radiation pressure. *Phys. Rev. Lett.* 24:156–159.

Ashkin, A., J. M. Dziedzic, J. E. Bjorkholm, and S. Chu. 1986. Observation of a single-beam gradient force optical trap for dieletric particles. *Optics Lett.* 11: 228–290.

Ashkin, A., J. M. Dziedzic, and T. Yamane. 1987. Optical trapping and manipulation of single cells using infrared-laser beams. *Nature (Lond.).* 330:769–771.

Ashkin, A., K. Schütze, J. M. Dziedzic, U. Euteneuer, and M. Schliwa. 1990. Force generation of organelle transport measured *in vivo* by an infrared laser trap. *Nature (Lond.).* 348:346–347.

Berg, H. 1983. Random Walks in Biology. Princeton University Press, Princeton, NJ. 11–12.

Berns, M. W., W. H. Wright, and R. W. Steubing. 1991. Laser microbeam as a tool in cell biology. *Int. Rev. Cytol.* 129:1–44.

Berns, M. W., W. H. Wright, B. J. Tromberg, G. A. Profeta, and J. J. Andrews. 1989. Use of a laser-induced optical force trap to study chromosome movement on the mitotic spindle. *Proc. Natl. Acad. Sci. USA.* 86:4539–4543.

Block, S. M. 1992. Making light work with optical tweezers. *Nature (Lond.).* 360:493–495.

Block, S. M., L. S. B. Goldstein, and B. J. Schnapp. 1990. Bead movement by single kinesin molecules studied with optical tweezers. *Nature (Lond.).* 348: 348–352.

Bray, D., J. Heath, and D. Moss. 1986. The membrane-associated 'cortex' of animal cells: its structure and mechanical properties. *J. Cell Sci. Suppl.* 4:71–88.

De Brabander, M., G. Geuens, R. Nuydens, M. Moeremans, and J. De Mey. 1985. Probing microtubule-dependent intracellular motility with nanometre particle video ultramicroscopy (nanovid ultramicroscopy). *Cytobios.* 43:273–283.

De Brabander, M., R. Nuydens, G. Geuens, M. Moeremans, and J. De Mey. 1986. The use of submicroscopic gold particles combined with video contrast enhancement as a simple molecular probe for the living cell. *Cell Motil. Cytoskeleton.* 6:105–113.

De Brabander, M., R. Nuydens, H. Geerts, and C. R. Hopkins. 1988. Dynamic behavior of the transferrin receptor followed in living epidermoid carcinoma (A431) cells with nanovid microscopy. *Cell Motil. Cytoskeleton.* 9:30–47.

De Brabander, M., R. Nuydens, A. Ishihara, B. Holifield, K. Jacobson, and H. Geerts. 1991. Lateral diffusion and retrograde movements of individual cell surface components on single motile cells observed with nanovid microscopy. *J. Cell Biol.* 112:111–124.

den Hartigh, J. C., P. M. P. van Bergen en Henegouwen, A. J. Verkleij, and J. Boonstra. 1992. The EGF receptor is an actin-binding protein. *J. Cell Biol.* 119:349–355.

Edidin, M., S. C. Kuo, and M. P. Sheetz. 1991. Lateral movements of membrane glycoproteins restricted by dynamic cytoplasmic barriers. *Science (Wash. DC).* 254:1379–1382.

Edidin, M., and I. Stroynowski. 1991. Differences between the lateral organization of conventional and inositol phospholipid-anchored membrane proteins. A further definition of micrometer scale domains. *J. Cell Biol.* 112: 1143–1150.

Edidin, M., M. C. Zúñiga, and M. P. Sheetz. 1994. Truncation mutants define and locate cytoplasmic barriers to lateral mobility of membrane glycoproteins. *Proc. Natl. Acad. Sci. USA.* 91:3378–3382.

Finer, J. T., R. M. Simmons, and J. A. Spudich. 1994. Single myosin molecule mechanics: piconewton forces and nanometre steps. *Nature (Lond.).* 368: 113–119.

Geerts, H., M. De Brabander, R. Nuydens, S. Geuens, M. Moeremans, J. De Mey, and P. Hollenbeck. 1987. Nanovid tracking: a new automatic method for the study of mobility in living cells based on colloidal gold and video microscopy. *Biophys. J.* 52:775–782.

Geerts, H., M. De Brabander, and R. Nuydens. 1991. Nanovid microscopy. *Nature (Lond.).* 351:765–766.

Gelles, J., B. J. Schnapp, and M. P. Sheetz. 1988. Tracking kinesin-driven movements with nanometre-scale precision. *Nature (Lond.).* 331:450–453.

Gonclaves, E., K. Yamada, H. S. Thatte, J. M. Backer, D. E. Golan, C. R. Kahn, and S. E. Shoelson. 1993. Optimizing transmembrane helicity accelerates insulin receptor internalization and lateral mobility. *Proc. Natl. Acad. Sci. USA.* 90:5762–5766.

Ghosh, R. N., and W. W. Webb. 1994. Automated detection and tracking of individual and clustered cell surface low density lipoprotein receptor molecules. *Biophys. J.* 66:1301–1318.

Hiramoto, Y. 1980. Rheological properties of sea urchin eggs. *Biorheology.* 6: 201–234.

Jacobson, K., A. Ishihara, and R. Inman. 1987. Lateral diffusion of proteins in membranes. *Annu. Rev. Physiol.* 49:163–175.

Kishino, A., and T. Yanagida. 1988. Force measurements by micromanipulation of a single actin filament by glass needles. *Nature (Lond.).* 334:74–76.

Kucik, D. F., E. L. Elson, and M. P. Sheetz. 1989. Forward Transport of Glycoproteins on Leading Lamellipodia in Locomoting Cells. *Nature (Lond.).* 340: 315–317.

Kucik, D. F., S. C. Kuo, E. L. Elson, and M. P. Sheetz. 1991. Preferential attachment of membrane glycoproteins to the cytoskeleton at the leading edge of lamella. *J. Cell Biol.* 114:1029–1036.

Kuo, S. C., and M. P. Sheetz. 1992. Optical tweezers in cell biology. *Trends Cell Biol.* 2:116–118.

Kusumi, A., Y. Sako, and M. Yamamoto. 1993. Confined lateral diffusion of membrane receptors as studied by single particle tracking (nanovid microscopy). Effects of calcium-induced differentiation in cultured epithelial cells. *Biophys. J.* 65:2021–2040.

Lee, G. M., F. Zhang, A. Ishihara, C. L. McNeil, and A. Jacobson. 1993. Unconfined lateral diffusion and an estimate of pericellular matrix viscosity revealed by measuring the mobility of gold-tagged lipids. *J. Cell Biol.* 120: 25–35.

Mecham, R. P., L. Whitehouse, M. Hay, A. Hinek, and M. P. Sheetz. 1991. Ligand affinity of the 67-kD elastin/laminin binding protein is modulated by the protein's lectin domain: visualization of elastin/laminin-receptor complexes with gold-tagged ligands. *J. Cell Biol.* 113:187–194.

Miller, K., M. Shipman, I. S. Trowbridge, and C. R. Hopkins. 1991. Transferrin receptors promote the formation of clathrin lattices. *Cell.* 65:621–631.

Nagle, J. F. 1992. Long tail kinetics in biophysics? *Biophys. J.* 63:366–370.

Oosawa, F. 1977. Actin-actin bond strength and the conformational change of F-actin. *Biorheology.* 14:11–19.

Pink, D. A. 1985. Protein lateral movement in lipid bilayers. Simulation studies of its dependence upon protein concentration. *Biochim. Biophys. Acta.* 818: 200–204.

Qian, H., M. P. Sheetz, and E. Elson. 1991. Single particle tracking (analysis of diffusion and flow in two-dimensional systems). *Biophys. J.* 60:910–921.

Saffman, P. G., and M. Delbrück. 1975. Brownian motion in biological membranes. *Proc. Natl. Acad. Sci. USA.* 72:3111–3113.

Sako, Y., A. Nagafuchi, M. Takeichi, and A. Kusumi. 1992. Intracellular regulation of the movements of E-cadherin on the cell surface. *Mol. Biol. Cell.* 3: 219a.

Sako, Y., and A. Kusumi. 1994. Compartmentalized structure of the plasma membrane for lateral diffusion of receptors as revealed by nanometer-level motion analysis. *J. Cell Biol.* 125:1251–1264.

Saxton, M. J. 1987. Lateral diffusion in an archipelago (the effect of mobile obstacles). *Biophys. J.* 52:989–997.

Saxton, M. J. 1989*a*. Lateral diffusion in an archipelago. Distance dependence of the diffusion coefficient. *Biophys. J.* 56:615–622.

Saxton, M. J. 1989*b*. The spectrin network as a barrier to lateral diffusion in erythrocytes. A percolation analysis. *Biophys. J.* 55:21–28.

Saxton, M. J. 1990. The membrane skeleton of erythrocytes. A percolation model. *Biophys. J.* 57:1167–1177.

Saxton, M. J. 1993. Lateral diffusion in an archipelago. Single-particle diffusion. *Biophys. J.* 64:1766–1780.

Schmidt, C. E., A. F. Horwitz, D. A. Lauffenburger, and M. P. Sheetz. 1993. Integrin-cytoskeletal interactions in migrating fibroblasts are dynamic, asymmetric, and regulated. *J. Cell Biol.* 123:977–991.

Schnapp, B. J., J. Gelles, and M. P. Sheetz. 1988. Nanometer-scale measurement using video light microscopy. *Cell Motil. Cytoskeleton.* 10:47–53.

Sheetz, M. P., S. Turney, H. Qian, and E. L. Elson. 1989. Nanometre-level analysis demonstrates that lipid flow does not drive membrane glycoprotein movements. *Nature (Lond.).* 340:284–288.

Sheetz, M. P. 1993. Glycoprotein mobility and dynamic domains in fluid plasma membranes. *Annu. Rev. Biophys. Biomol. Struct.* 22:417–431.

Svoboda, K., and Block, S. M. 1994. Force and velocity measured for single kinesin molecules. *Cell.* 77:773–784.

Takeuchi, M., H. Miyamoto, H. Komizu, and A. Kusumi. 1992. Atomic force microscopy (AFM) observation of the membrane skeleton network: comparison with electron microscopy. *Cell Struct. Funct.* 17:487a.

Tsuda, K., Y. Sako, and A. Kusumi. 1992. Interaction between integral membrane proteins and the membrane skeleton in human erythrocyte as studied by nanometer-level analysis of movements. *Cell Struct. Funct.* 6:487a.

Tsuji, A., K. Kawasaki, S. Ohnishi, H. Merkle, and A. Kusumi. 1988. Regulation of band 3 mobilities in erythrocyte ghost membranes by protein association and cytoskeletal meshwork. *Biochemistry.* 27:7447–7452.

Tsuji, A., and S. Ohnishi. 1986. Restriction of the lateral motion of band 3 in the erythrocyte membrane by the cytoskeletal network: dependence on spectrin association state. *Biochemistry.* 25:6133–6139.

Vale, R. D., and E. M. Shooter. 1983. Conversion of nerve growth factor-receptor complexes to a slowly dissociating, triton X-100 insoluble state by anti nerve growth factor antibodies. *Biochemistry.* 22:5022–5028.

Waugh, R. E. 1982. Temperature dependence of the yield shear resultant and the plastic viscosity coefficient of erythrocyte membrane. *Biophys. J.* 39:273–278.

Weber, G., and K. O. Greulich. 1992. Manipulation of cells, organelles, and genomes by laser microbeam and optical trap. *Int. Rev. Cytol.* 133:1–41.

Wiegant, F. A. C., F. J. Blok, L. H. K. Defize, W. A. M. Linnemans, A. J. Verkley, and J. Boonstra. 1986. Epidermal growth factor receptors associated to cytoskeletal elements of epidermoid carcinoma (A431) cells. *J. Cell Biol.* 103:87–94.

Wier, M., and M. Edidin. 1988. Constraint of the translational diffusion of a membrane glycoprotein by its external domains. *Science (Wash. DC).* 242: 412–414.

Yechiel, E., and M. Edidin. 1987. Micrometer-scale domains in fibroblast plasma membranes. *J. Cell Biol.* 105:755–760.

Zippel, R., L. Morello, R. Brambilla, P. M. Comoglio, L. Alberghina, and E. Sturani. 1989. Inhibition of phosphotyrosine phosphatases reveals candidate substrates of the PDGF receptor kinase. *Eur. J. Cell Biol.* 50:428–434.